Article

Not peer-reviewed version

Assessment of Spatiotemporal Wind Complementarity

Dirk Schindler *, Jonas Wehrle, Leon Sander, Christopher Schlemper, Kai Bekel, Christopher Jung

Posted Date: 30 June 2025

doi: 10.20944/preprints202506.2335.v1

Keywords: wind energy; wind energy expansion; variable renewable energy sources; wavelet analysis; singular value decomposition

 doi:10.20944/preprints202506.2335.v1

Article

Assessment of Spatiotemporal Wind Complementarity

Dirk Schindler [1,*] Jonas Wehrle [1], Leon Sander [1], Christopher Schlemper [2], Kai Bekel [2] and Christopher Jung [1]

[1] Environmental Meteorology, University of Freiburg, Werthmannstrasse 10, D-79085 Freiburg, Germany

[2] Das Grüne Emissionshaus, Goethestrasse 4, D-79100 Freiburg, Germany

* Correspondence: dirk.schindler@meteo.uni-freiburg.de; Tel.: +49-761-203-3588

Abstract

This study investigates whether combining singular value decomposition with wavelet analysis can provide new insights into the spatiotemporal complementarity between wind turbine sites, surpassing previous findings. Earlier studies predominantly relied on various forms of correlation analysis to quantify complementarity. While correlation analysis offers a way to compute global metrics summarizing the relationship between entire time series, it inherently overlooks localized and time-specific patterns. The proposed approach overcomes these limitations by enabling the identification of spatially explicit and temporally resolved complementarity patterns across a large number of wind turbine sites in the study area. Because complementarity information is derived from orthogonal components obtained through singular value decomposition of a wind power density matrix, there is no need to adjust for phase shifts between sites. Moreover, the complementary contributions of these components to overall wind power density are expressed in watts per square meter, directly reflecting the magnitude of the analyzed data. This facilitates a site-specific, complementarity-optimized strategy for further wind energy expansion.

Keywords: wind energy; wind energy expansion; variable renewable energy sources; wavelet analysis; singular value decomposition

1. Introduction

Wind power is subject to fluctuations across various spatial and temporal scales. This spatiotemporal variability is caused by differences in large-scale airflow regimes, which are superimposed by regional and local circulations. As a result, the wind speed (*WS*) variation near the ground ranges from less than a second to several decades [1–3].

The influences of airflow regimes are reflected in complex time series of wind speed, which are composed of multiple components [4]. Among the components that shape the spatiotemporal variability of wind speed are the daily cycle [5], components associated with weather changes [6–8], seasonal components reflecting intra-annual variability [5,9], interannual variability [2,10,11], and long-term changes quantified as trend components [12–15], as well as components that cannot be attributed to any determinism [16].

The proportions and characteristics of the different time series components are not the same across the globe [17]. They vary regionally. While wind speed time series in the tropics are dominated by a daily cycle, outside the tropics, wind speed time series are typically characterized by a pronounced annual cycle. For example, in Europe, wind speed time series are largely shaped by an annual cycle that peaks in winter, primarily due to the intensified westerlies prevailing in the Northern Hemisphere during that season [11]. As summer approaches, mean wind speed decreases significantly.

 doi:10.20944/preprints202506.2335.v1

While large-scale atmospheric flow regimes determine the overarching spatiotemporal characteristics of the European wind resource, the continent's geographic extent means it is simultaneously influenced by multiple weather patterns which are among the main drivers of spatiotemporal variability in wind resources [18,19]. These regimes not only exert a strong influence on the day-to-day variability of wind speed across Europe but also modulate the intra-annual variation of wind power availability [11].

In the context of wind energy utilization, complementarity refers to the interplay of wind conditions at different sites or times, where fluctuations in wind availability balance each other out [20,21]. This means that when wind power is low at one location and little electricity is generated, complementary sites may have high wind availability and generate more power – and vice versa.

The types of complementarity among renewable energies are referred to as spatial complementarity, which arises from the fact that different regions and sites have varying wind resources. Another is temporal complementarity, which results from sub-hourly, hourly, daily, multi-day, or seasonal differences in the availability of wind resources. When spatial and temporal complementarity are considered together, this is referred to as a spatiotemporal analysis of complementarity [22].

It has been proposed to use wind energy in a complementary way because the spatiotemporal variability of wind power generation leads to supply shortage [23,24], electricity surplus [25], and poses a barrier to maintaining a consistently high share of wind energy in the electricity mix [26–30].

Among the approaches reviewed to reduce wind resource variability through complementary use [31], cross-border and interregional utilization of wind energy has been proposed to smooth regional and local fluctuations. The potential to mitigate multi-day variability of wind resources in Europe – driven by changing weather patterns – has been demonstrated by either installing wind turbines in regions with contrasting weather regimes or distributing them across Europe's peripheral areas [32].

Various methods and metrics were used to determine the complementarity between renewable energy sources like wind, solar, hydro, and biomass. In most cases, the complementarity between wind and solar energy was quantified by different types of correlation coefficients. Among the applied coefficients are the Pearson correlation coefficient [5,9,11,33–46], the Spearman correlation coefficient [47–52], and the Kendall correlation coefficient [52–66].

The Pearson correlation coefficient measures linear co-movement, regardless of scale. The Spearman and Kendall correlation coefficients measure monotonic co-movement, considering the rank order of values. None of these coefficients directly capture the magnitude of differences and the dependence structure between different variables [67].

Cantor et al. [68] summarized issues that arise from the use of correlation coefficients in the quantification of complementarity. These include, among others, that negative correlation coefficient values do not always imply complementarity, that the magnitude of the correlated quantities matters, and that correlation coefficients are limited to the comparison of two time series.

Interpreting the correlation results reported for wind complementarity is often challenging. In many cases, the reported values of the correlation coefficients fluctuate between -0.5 and 0.0 on time scales ranging from minutes to days [35,59], indicating weak to no correlation. Lower correlation coefficient values up to -0.9 were reported for monthly wind-solar complementarity across Europe [69]. In any case, correlation does not allow for a temporally localized interpretation of the results.

Other commonly applied approaches to determining complementarity include variation-based indices [45,53,56,68,70,71], copula-based correlation methods [11,52,65,72,73], and approaches that additionally apply normalization to enhance the comparability of time series [35,63,65,66,71].

These methods have been proposed to optimize various aspects of wind energy utilization. This includes the selection and interconnection of complementary wind power plant sites [74], the planning of hybrid power systems, such as wind-solar [75], wind-solar-hydro [35], and wind-hydro-biomass combinations [76], the stabilization of wind power feed-in [77], the reduction of grid congestion [78,79], and curtailment [80]. The stabilization of wind power feed-in through reduction

 doi:10.20944/preprints202506.2335.v1

of spatiotemporal wind power variability leads to a more continuous electricity supply, which improves grid operation and management [81].

Building on previous approaches—which are limited in their ability to quantify wind resource complementarity in large wind turbine fleets due to the complex, nonlinear superposition of various wind time series components—this study investigates whether combining singular value decomposition (SVD) and spectral methods [82], such as Fourier [83] and wavelet analysis [4], can yield new insights into wind resource complementarity in large turbine fleets by identifying dominant wind patterns and their variability.

The tested hypothesis is that by reducing the dimensionality in the wind power density (*WPD*) time series, essential structures are summarized in a small number of components, making global and latent patterns in the data visible that cannot be revealed through pairwise comparisons between wind turbine sites. The component matrices are intended to enable the visualization of complex interrelationships that remain hidden when using large similarity matrices from pairwise comparisons. The aim of the study is to find wind turbines sites that provide complementary contributions to wind energy generation at times when other wind power plants deliver little or no output.

Germany is chosen as the study area for this novel approach because, compared to many other countries, it has a large off- and onshore wind turbine fleet and long-term, hourly resolved wind speed (*WS*) data from the Wind Speed Complementarity Model (WiCoMo) are available at a very high spatial resolution [44].

2. Materials and Methods

2.1. Study Area and Wind Speed Data

The study area Germany covers about 357,000 km² and its wind turbine fleet includes both offshore and onshore wind turbines. The analysis incorporates 29,807 actual wind turbine sites, of which 1,664 sites are offshore – mostly grouped in wind farms.

Since operational data from wind turbines are considered trade secrets and therefore not available for a comprehensive complementarity analysis, WiCoMo output was used for this study. WiCoMo is a three-dimensional statistical-empirical model that provides hourly *WS* data on a 25 m × 25 m grid for Germany [44].

The analysis period covers ten years, from 1 January 2015 to 31 December 2024. Since the analysis also included the calculation of mean annual cycles, wind speed values from 29 February 2016, 2020, and 2024, were removed. As a result, a matrix with dimensions of 87,600 (hourly values) × 29,807 (wind turbine sites) wind speed values was available for analysis.

In addition to the WiCoMo validation described in a previous study [44], which was based on data from 508 measurement stations of the German Meteorological Service, an operator of wind turbines provided hourly operational data for 83 turbines grouped at 12 sites. These data were used to strengthen the significance of the following results. The validation was carried out for the period 2017-2021 and yielded results for the mean absolute error of $MAE = 0.50$ (mean value) ± 0.33 (standard deviation) W/m² and a Pearson correlation coefficient of $R = 0.91 \pm 0.02$.

The distribution of wind turbines within the study area is shown in Figure 1a. Wind turbine density is highest in the northwest and west, decreasing towards the east and south. The mean wind power density (WPD_{mean}), calculated from WiCoMo output for the study period, is presented in Figure 1b. It shows that the highest WPD_{mean} values at 100 m above ground, reaching up to 575 W/m², are achieved by offshore wind turbines in the North Sea and Baltic Sea. Further south, WPD_{mean} values are generally lower, down to 40 W/m², due to increased surface roughness and greater distance from the coast. Only at higher-elevation sites, mostly in low mountain ranges, are similarly high WPD_{mean} values observed as those found near the coast onshore.

Preprints.org (www.preprints.org) | NOT PEER-REVIEWED | Posted: 30 June 2025 doi:10.20944/preprints202506.2335.v1

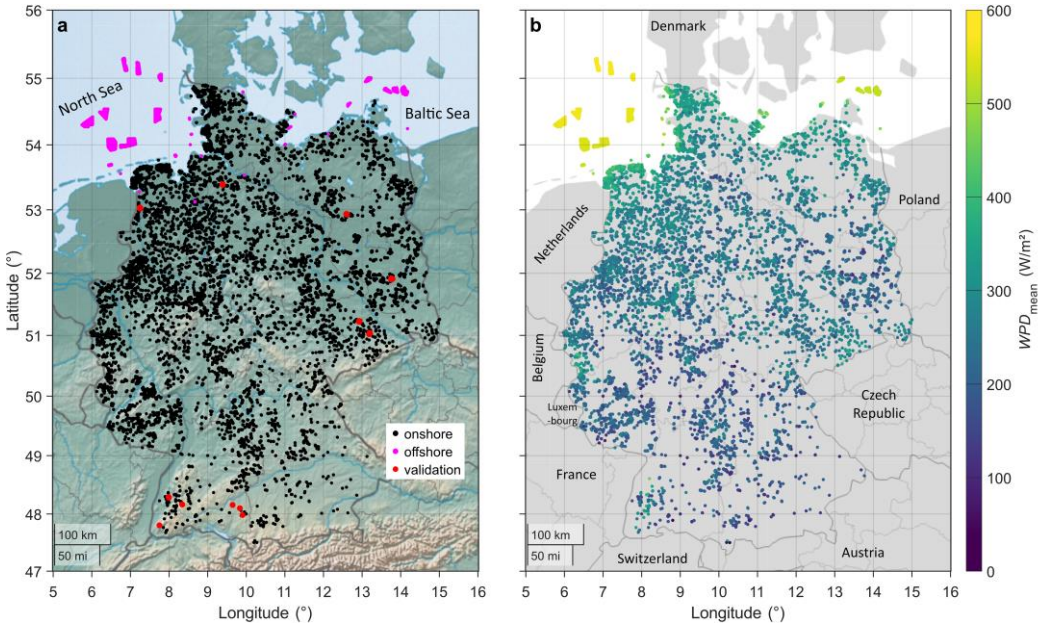

Figure 1. (a) Study area with sites of offshore (pink dots) and onshore (black dots) wind turbines. Red dots indicate 12 wind turbine sites where hourly Wind Speed Complementarity Model (WiCoMo) results were validated using 83 hourly wind speed time series measured directly at wind turbines. **(b)** Mean wind power density (WPD_{mean}) at 100 m above ground 2015-2024 at 29,807 wind turbine sites as calculated with WiCoMo [44].

To investigate wind spatiotemporal complementarity within the study area, the following main steps were carried out (Figure 2): (1) Calculation of *WPD* from hourly wind speed data at actual wind turbine sites; (2) application of SVD to the *WPD* matrix (dimensions 87,600 × 29,807); (3) computation of the spatial (*Sp*) and temporal (*Te*) information derived from the SVD components; (4) derivation of spatial and temporal complementarity from *Sp* and *Te*; (5) quantification of spatiotemporal wind complementarity at different scales; (6) execution of wavelet analysis to identify dominant time scales in the SVD components.

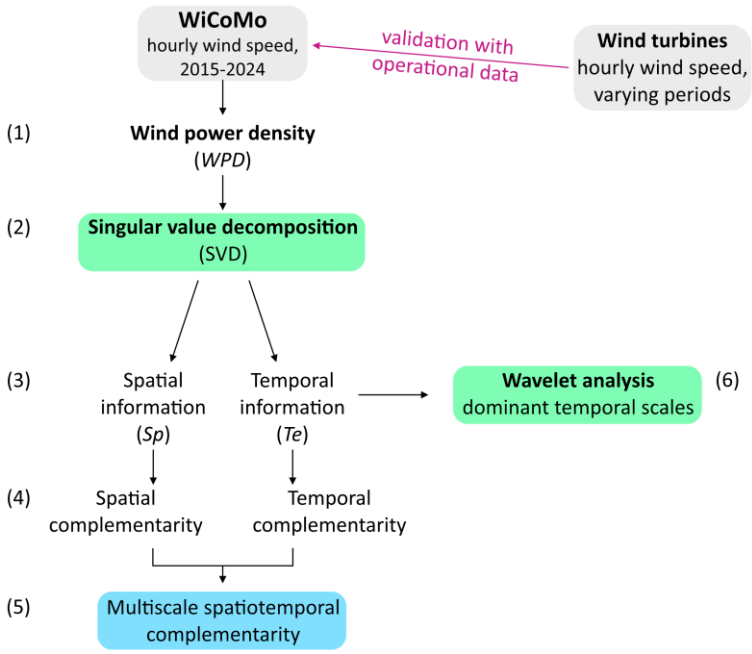

 doi:10.20944/preprints202506.2335.v1

Figure 2. Flowchart illustrating the main processing steps for the analysis and quantification of wind spatiotemporal complementarity in the study area 2015-2024.

2.2. Analysis of Wind Complementarity

Wind power density was calculated from hourly wind speed at 100 m altitude (WS_{100m}) at the actual wind turbine sites. To minimize the influence of wind turbine characteristics on the analysis of complementarity, a uniform hub height of 100 m was used for all analyzed sites:

$$WPD = \frac{1}{2} \cdot \rho \cdot WS_{100m}^3 \quad (1)$$

where ρ is the air density kept constant at a value of 1.225 kg/m³ [11]. WPD_{mean} in the study area was calculated from all *WPD* time series.

For all hours with the wind turbine location-specific $WS_{100m} > 25$ m/s, WS_{100m} is set to 0 m/s to account for wind turbine shutdown due to excessive wind loading.

The *WPD* calculation was then restricted to 3 m/s ≤ WS_{100m} ≤ 12 m/s, representing the typical cut-in and rated speed range and considered turbine saturation effects. This restriction resulted in maximum hourly *WPD* values of 1,058.4 W/m².

The complementarity between the analyzed wind turbine sites was assessed based on SVD [84] of the *WPD* matrix consisting of 87,600 hourly *WPD* values and 29,807 location-specific *WPD* time series:

$$WPD = U \cdot S \cdot V^T = \sum_{j=2}^{10} s_j \cdot u_j \cdot v_j^T \quad (2)$$

where *S* is a diagonal matrix with singular values *s*. The columns of *U* represent the left singular vectors (temporal modes) of the SVD components (*u*); the columns of *V* contain the right singular vectors, i.e., the spatial component-specific modes (*v*). V^T is the Hermitian transpose of *V*.

The *WPD* matrix was decomposed into *j* = 2, …, 10 orthonormal (orthogonal and normalized to a length of 1) and independent components to gain an overview of the distribution of explained variance (*EV*) across the components. The component-specific EV_k (*k* = 1, …, 10) was calculated as

$$EV_k = \frac{s_k^2}{\sum s_k^2} \cdot 100. \quad (3)$$

To enable meaningful interpretation of the orthonormal SVD components, the singular vectors were multiplied by the corresponding singular values. As a result, they are no longer normalized but remain orthogonal and independent from one another.

Based on the EV_k values (*k* = 2, …, 10), the most suitable number of SVD components for analyzing wind complementarity was determined. The key criteria were the *EV* distribution across the components and the spatial patterns revealed by the components within the study area.

The spatial pattern *Sp* associated with the SVD components were analyzed as

$$Sp_k = s_k \cdot v_k. \quad (4)$$

The spatial complementarity (SpC_k) of $Sp_k(i)$ for $k > 1$ with $Sp_1(i)$ ($SpC_k(i)$) was assessed as

$$SpC_k(i) = \begin{cases} Sp_k(i), & if\ sign(Sp_k(i) \neq Sp_1(i)) \\ 0 \end{cases}, \quad (5)$$

where *i* = 1, …, 29,807 and represents the analyzed wind turbine sites.

The temporal structure *Te* of the SVD components was determined as

$$Te_k = s_k \cdot u_k. \quad (6)$$

Regardless of the number of components, Te_1 is non-negative due to the non-negative nature of *WPD*. It contains a consistently positive *WPD* pattern that largely aligns with known physical processes. Its contribution to total *WPD* can be meaningfully expressed in absolute units (i.e. W/m²).

 doi:10.20944/preprints202506.2335.v1

All other Te_k, with $k > 1$, contain both positive and negative values. These values do not represent independent energy sources but indicate deviations from the dominant pattern. Specifically, they describe

- amplifications of Te_1 in certain time periods and wind power density exceeds what is explained by Te_1 alone (positive contributions),
- attenuations of Te_1 at other times and wind power density is reduced compared to Te_1 (negative contributions).

These characteristics are physically meaningful, as near-surface wind fields inherently exhibit complex spatiotemporal patterns that can lead to simultaneous amplifications and attenuations, e.g., due to local pressure systems or terrain. The amplification of $Te_1 = Te_{1,pos}$ by $Te_{k,pos}$ ($k > 1$) is interpreted as complementary boost of Te_1.

The sum of $Te_{k,pos}$ was equated to the magnitude of the original data to quantify the contributions of the wind turbine sites in W/m² to the total sum of *WPD* in the study area:

$$\sum_{k=1}^{K} Te_{k,pos} \coloneqq WPD \tag{7}$$

where *K* is the total number of SVD components.

The quantification of the SVD component-specific contributions ($C_k(i,t)$, t is the time) to *WPD* follows the approach

$$C_k(i,t) = \frac{Te_{k,pos}(i,t)}{\sum_{j=1}^{K} Te_{j,pos}(i,t)} \cdot WPD(i,t) \tag{8}$$

The procedure used to calculate *WPD* from the WiCoMo data and to decompose the resulting *WPD* matrix was repeated for the measured 83 wind speed time series available from the 12 wind turbine sites used for additional validation. The SVD components from these measured time series were compared to the SVD components obtained from the decomposition of the WiCoMo matrix.

The continuous wavelet transform [85] was used to obtain information about the time-frequency content of Te_k:

$$W_k(a,b) = \int_{-\infty}^{\infty} Te_k(t) \cdot \psi_{a,b}^{*}(t) \cdot dt \tag{9}$$

where *W* are the SVD component-specific wavelet coefficients available as complex numbers, *a* is the scale factor, which defines the frequency of the wavelet function, *b* is the translation factor indicating the position of the wavelet on the time (*t*) axis, ψ is the mother wavelet function (analytic Morlet wavelet), and the * indicates the complex conjugate.

The wavelet coefficients were calculated for *a* = 1, …, 448 scales, producing information on the time-frequency behavior of the SVD components from 2 hours to 3.7 years. The real part of W_k $\left(Re_k(a)\right)$ represents the scale-specific temporal course of the wavelet coefficients in the study period.

Wavelet variance spectra (VS_k) were then calculated from W_k [86]:

$$VS_k(a) = \frac{1}{N}\sum_b |W_k(a,b)|^2, \tag{10}$$

where $N = 448$ is the number of scales. As VS_k differs greatly in magnitude, they were normalized to [0,1] for better comparability.

All calculations and analyses were performed with the Matlab 2024b software (The Mathsworks Inc., Natick, Massachusetts, United States).

3. Results and Discussion

3.1. Singular Value Decomposition of Wind Power Density Matrix

Using only two components ($k = 2$) did not sufficiently capture the spatial *WPD* variability. The first component accounted for more than 94 % of *EV*, making it overly dominant. Starting from a

 doi:10.20944/preprints202506.2335.v1

decomposition of the *WPD* matrix into five or more components (k = 5, …, 10), the spatial *WPD* patterns became highly fragmented and were shaped by small-scale, local characteristics, which were associated with EV_k values of less than 1.0 %.

Since the decomposition into four components (k = 4) accounted for the wind energy sites located in the low mountain ranges in the central and southern parts of the study area, this decomposition was preferred over the three-component version (k = 3) for further analysis. The decomposition into three components failed to identify productive sites in the low mountain ranges common in the study area, as the three components primarily represented sites in the northern parts.

The EV_k values associated with the four components are shown in Figure 3a, and the cumulative values ($\sum EV_k$) are presented in Figure 3b. These figures reveal that the first SVD component, with a share of 89.1 %, dominates the spatiotemporal *WPD* pattern at the analyzed wind turbine sites. The shares of explained variance for the subsequent components are significantly lower: 5.5 % for the second component, 3.6 % for the third, and 1.7 % for the fourth.

3.2. Temporal Structure of Wind Power Density

The first SVD component, which explains the largest share of variance in the *WPD* matrix, is dominated by the annual cycle of WS_{100m}, which largely determines the wind energy availability across Central Europe [8,11,32]. The annual cycle is well represented by the real part (Re_1) of the coefficients at scale a = 388 resulting from the wavelet transform of Te_1 (Figure 3a). The units on both axes are arbitrary to allow comparability between the different quantities. All values of Te_1 and Re_1 are positive.

This non-negative property of Te_1 does not apply to Te_2 (Figure 3b) through Te_4 (Figure 3d), which fluctuate around the zero line and thus also take on negative values (green lines). The positive values (blue lines) of Te_2 to Te_4 are interpreted as amplifying contributions to Te_1, since Te_2 to Te_4 are, by definition, orthogonal – and thus independent – from Te_1. This amplification is considered a complementary contribution. The negative values of Te_2 to Te_4 attenuate the expression of Te_1 and cannot contribute to complementarity.

In Figure 3d, in addition to Te_4, the real part of Te_4 (Re_4) combined with the wavelet scale a = 148 is also shown. This wavelet scale corresponds to a time scale of 48 hours, which reflects a typical frequency of weather changes in Europe [6–8,18]. As a result, it exhibits significantly higher-frequency fluctuations compared to the wavelet scale used to approximate the annual cycle of Te_1.

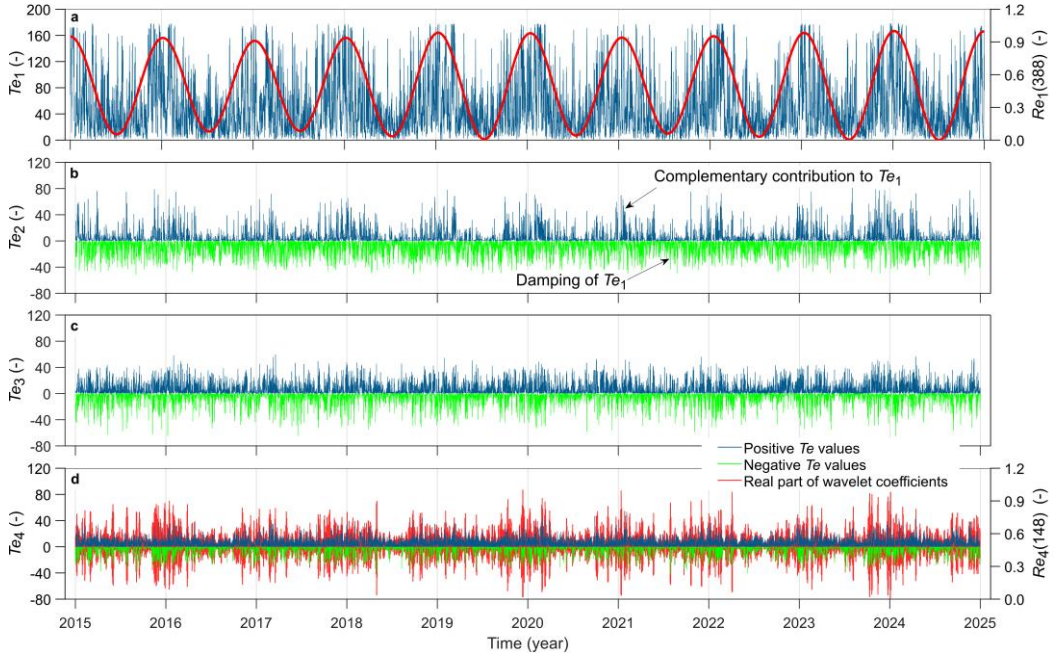

 doi:10.20944/preprints202506.2335.v1

Figure 3. Temporal structure of the (**a**) first wind power density (*WPD*) component (Te_1) from singular value decomposition (SVD) with the real part (Re_1) of the coefficients at scale a = 388 resulting from the wavelet transform of Te_1 from 2015 to 2024; (**b**) second *WPD* component (Te_2) from SVD; (**c**) third *WPD* component (Te_3) from SVD; (**d**) fourth *WPD* component (Te_4) from SVD with Re_4 of the coefficients at scale a = 148 resulting from the wavelet transform of Te_4.

The four *VS* calculated from Te_1 to Te_4 are shown in Figure 4. They reveal that Te_1 exhibits two distinct ranges with particularly high shares of variance: one corresponding to scales between half a week and several weeks, similar to the wavelet spectra presented in previous studies [87,88], and another associated with the annual cycle of wind speed [82,87].

In contrast, Te_2 shows significantly lower wavelet variance shares at the annual cycle scales compared to Te_1. Its highest variance contributions are found at scales ranging from several days to a few weeks.

Only very small shares of variance at the annual cycle scales are observed for Te_3 and Te_4. For these two components, the dominant scales lie between half a day and one week, indicating that their temporal variability is largely driven by weather changes**.**

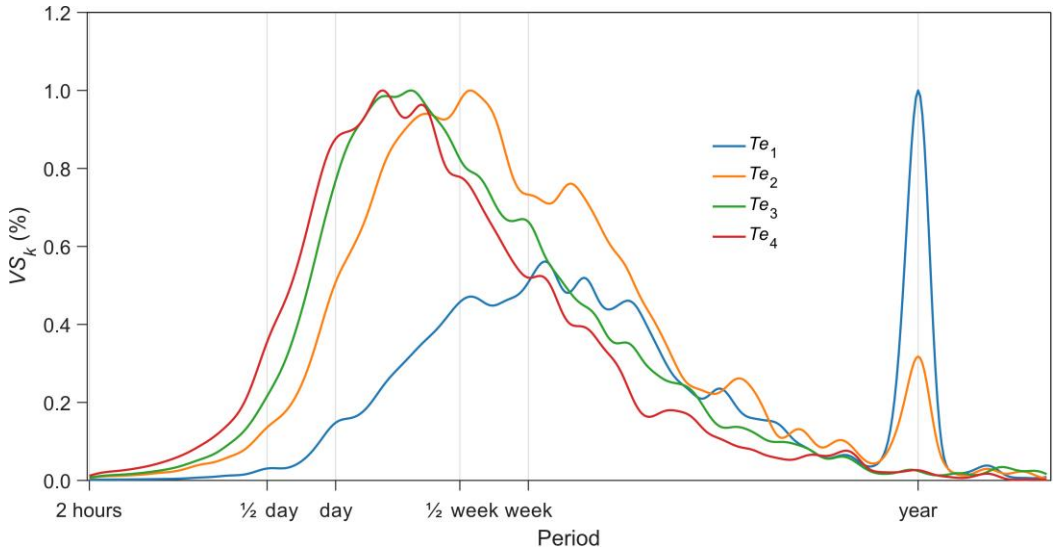

Figure 4. Normalized, rescaled to the range [0,1], wavelet variance spectra (VS_k) calculated over N = 448 scales for the temporal structure (Te_k, k = 1, …, 4) of four components resulting from the singular value decomposition (SVD) of the wind power density (*WPD*) matrix.

To illustrate the central tendencies of $Te_{1,\mathrm{pos}}$ to $Te_{4,\mathrm{pos}}$ throughout the year, Figure 5 shows their mean monthly daily cycles and their relative contributions to the sum of $Te_{1,\mathrm{pos}}$ through $Te_{4,\mathrm{pos}}$ ($\sum Te_{k,pos}$).

The mean monthly daily cycles of $Te_{1,\mathrm{pos}}$ show maximum values during the nighttime hours in all months (Figure 5a). During the daytime, its share decreases on average by between 2.8 % in December and 8.6 % in April. The shares of $Te_{1,\mathrm{pos}}$ are by far the highest throughout the year compared to $Te_{2,\mathrm{pos}}$ to $Te_{4,\mathrm{pos}}$. Over the study period, the average $Te_{1,\mathrm{pos}}$ share is 73.0 (mean) ± 2.5 % (standard deviation).

The pattern of reduced *WPD* during the day results from a marked wind speed decrease. Daytime wind speed during the summer months have been reported in earlier studies for the flat, northeastern part of the study area, showing a similar pattern [89,90]. This diurnal cycle is related to the development of the atmospheric boundary layer over flat land surfaces, transitioning from turbulent mixed conditions during the day to stable, weakly turbulent or even laminar flows at night. Particularly during the morning transition period, strong *WPD* gradients can occur.

 doi:10.20944/preprints202506.2335.v1

$Te_{2,\mathrm{pos}}$ shows significantly lower values (Figure 5b). Its average share over the study period is 5.6 %. Here as well, nighttime values are higher than daytime values in all months. The mean daily difference ranges from 1.8 % in September to 3.1 % in August. It is higher in the spring (March, April, May) and summer months (June, July, August) than in the fall (September, October, November) and winter months (December, January, February).

The daytime decreases in $Te_{1,\mathrm{pos}}$ and $Te_{2,\mathrm{pos}}$ are compensated by higher values of $Te_{3,\mathrm{pos}}$ (Figure 5c) and $Te_{4,\mathrm{pos}}$ (Figure 5d). These two components show their highest values during the day. The difference in the mean monthly daily values of $Te_{3,\mathrm{pos}}$ ranges from 1.6 % (December) to 5.8 % (August), showing a pronounced annual cycle. The average share of $Te_{3,\mathrm{pos}}$ over the study period is 9.5 ± 1.5 %. A similar pattern is found for $Te_{4,\mathrm{pos}}$. Its mean daily differences between day and night range from 2.2 % (January) to 6.0 % (April). With an average share of 11.9 ± 2.2 %, $Te_{4,\mathrm{pos}}$ contributes more than $Te_{3,\mathrm{pos}}$.

The patterns of $Te_{3,\mathrm{pos}}$ and $Te_{4,\mathrm{pos}}$, featuring a daytime *WPD* maximum, resemble the average diurnal cycle of wind speed during summer as presented in a previous study based on measurements from the southern part of the study area [90].

In addition to the mean monthly daily cycles, mean annual cycles are evident in $Te_{1,\mathrm{pos}}$ to $Te_{4,\mathrm{pos}}$. While $Te_{1,\mathrm{pos}}$ and $Te_{2,\mathrm{pos}}$ show the highest values in the winter months, when *WPD* also reaches its peak, $Te_{3,\mathrm{pos}}$ and $Te_{4,\mathrm{pos}}$ show the highest values in the summer months, indicating that their relative importance increases during the summer – when *WPD* is at a minimum across Europe – and decreases during the winter months, when the westerly flow in the northern hemisphere over Europe is strongest [91].

The corresponding values of the first component from the SVD decomposition of the 83 wind speed time series measured at wind turbines show a similar pattern to $Te_{1,\mathrm{pos}}$ and $Te_{3,\mathrm{pos}}$. In addition to the annual cycle, the average diurnal cycles of $Te_{1,\mathrm{pos}}$ and $Te_{3,\mathrm{pos}}$ are well represented for most months. Although the agreement between the evolution of $Te_{1,\mathrm{pos}}$, $Te_{3,\mathrm{pos}}$, and the SVD component from the validation dataset is not always exact – likely due to differences between the datasets – the observed similarity is remarkably high, especially considering the limited number of validation time series available.

Agreement with $Te_{2,\mathrm{pos}}$ is absent because there are no validation sites located within the $Te_{2,\mathrm{pos}}$ region, which implies that this region cannot be represented. Agreement with $Te_{4,\mathrm{pos}}$ is noticeable with respect to the annual cycle. However, the average monthly diurnal cycles differ, which can be attributed to the low number of validation sites within the $Te_{4,\mathrm{pos}}$ area, particularly in the Baltic Sea region.

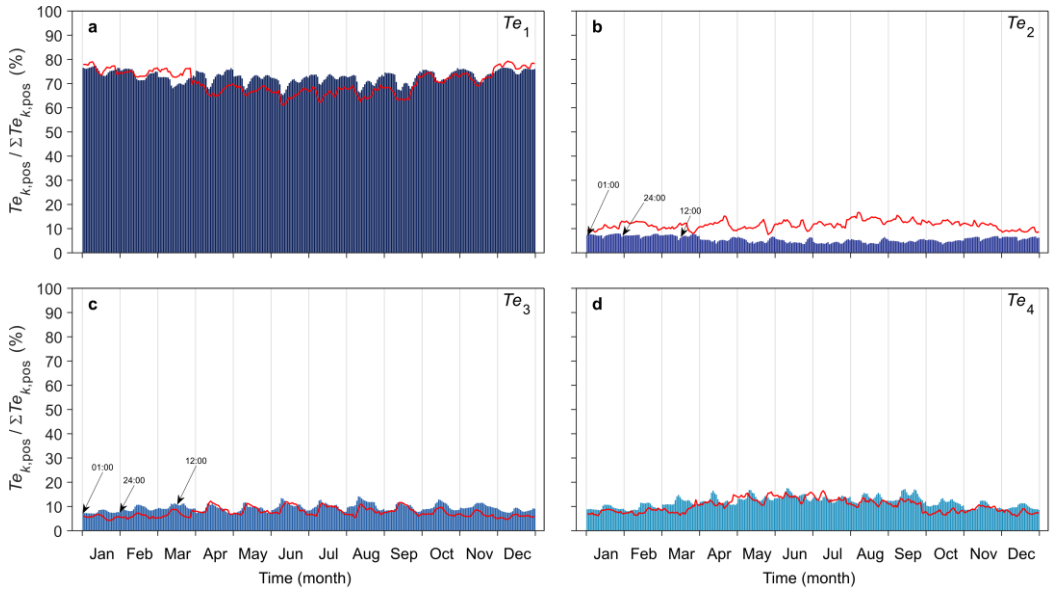

 doi:10.20944/preprints202506.2335.v1

Figure 5. Mean monthly daily cycles (1:00 to 24:00) of the share (in %) of positive temporal structure values ($Te_{k,pos}$, k = 1, …, 4) in the total temporal structure ($\sum Te_{k,pos}$) of wind power density (*WPD*) in the study area 2015-2024. (**a**) $Te_{1,pos}/\sum Te_{k,pos}$; (**b**) $Te_{2,pos}/\sum Te_{k,pos}$; (**c**) $Te_{3,pos}/\sum Te_{k,pos}$ and (**d**) $Te_{4,pos}/\sum Te_{k,pos}$. The red lines represent the temporal structure of four components resulting from the singular value decomposition (SVD) of the *WPD* matrix available from 83 wind turbines.

The mean annual shares of $Te_{k,pos}$ are not always the same (Figure 6). They fluctuate from year to year over the study period, which is a consequence of the interannual *WPD* variability in Europe [2,92,93]. The largest fluctuations are observed for $Te_{1,pos}$, which also accounts for the greatest *WPD* share. The largest year-to-year change of $Te_{1,pos}$ occurs between 2015 and 2016, amounting to 13.5 %. Over the study period from 2015 to 2021, the range of annual $Te_{1,pos}$ values is approximately 15.2 %.

The ranges of year-to-year fluctuations are significantly smaller for $Te_{2,pos}$ (4.4 %), $Te_{3,pos}$ (2.0 %), and $Te_{4,pos}$ (0.9 %). This indicates that $Te_{1,pos}$ primarily reflects the interannual *WPD* variability and determines the general level of wind energy availability in the study area.

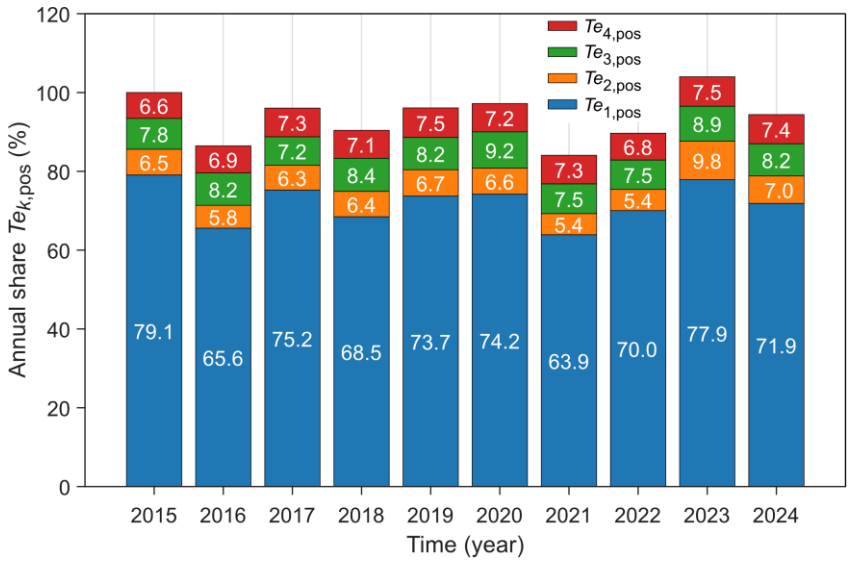

Figure 6. Mean annual shares of the positive values of the temporal structure of the singular value decomposition ($Te_{k,pos}$, k = 1, …4) from 2015 to 2024. For better comparability, the values were normalized to the values of the year 2015. This means that in 2015, the sum of the $Te_{k,pos}$ shares equals 100 %.

To illustrate the significance of $Te_{4,pos}$ for WPD_{mean} by example, Figure 7 shows the course of WPD_{mean} and $Te_{4,pos}/\sum Te_{k,pos}$ for the year 2023, which was the year with the highest WPD_{mean} values in 2015-2024.

During the winter months, when the large-scale westerly flow is most pronounced and $Te_{1,pos}$ dominates the structure of WPD_{mean}, the share of $Te_{4,pos}$ is lower in most hours compared to the summer months, when the westerly flow weakens. At such times, $Te_{4,pos}$ can contribute up to 60 % of the available WPD_{mean}, as illustrated by the inset for the months of May and June.

From this representation, it can be concluded that $Te_{1,pos}$ determines the general annual level of WPD_{mean}, but $Te_{2,pos}$ to $Te_{4,pos}$ make substantial contributions to WPD_{mean} at certain times. From the perspective of complementarity, wind turbine sites that contribute substantially to WPD during such periods are certainly an important complement to those where $Te_{1,pos}$ contributes little at the same time.

 doi:10.20944/preprints202506.2335.v1

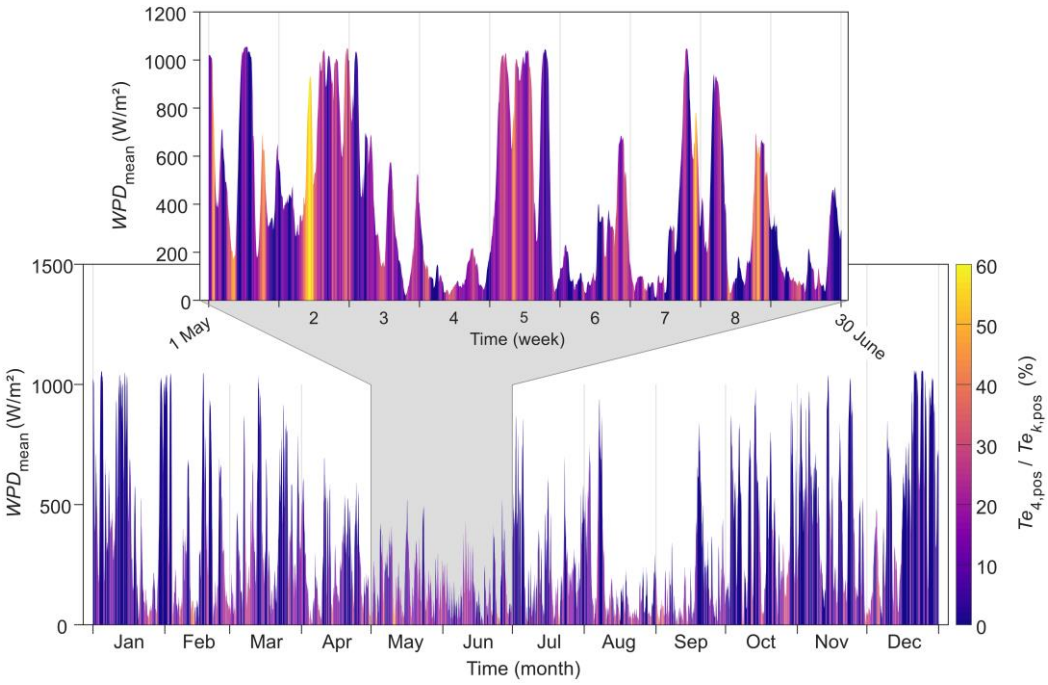

Figure 7. Hourly mean values of wind power density in the study area (WPD_{mean}) in the year 2023 together with the share of $Te_{4,pos}$ in the sum of $Te_{k,pos}$ with $k = 1, \ldots, 4$ $\left(Te_{4,pos}/\sum Te_{k,pos}\right)$. The inset highlights the course of both variables during May and June 2023.

3.3. Spatial Pattern of Wind Power Density

The spatial pattern associated with the four SVD components are shown in Figure 8. As the prevailing westerlies determine the spatial distribution of wind speed over Europe [32], dominant Sp_1 exhibits the highest *WPD* values at offshore sites and at near-coastal onshore sites in the northern parts of the study area.

Toward the east and south, *WPD* values decrease markedly (Figure 8a). A clearly discernible north-south gradient in *WPD* is revealed by Sp_2, with the northern sites showing the lowest *WPD* values. The highest *WPD* values occur in the southwest and central parts of the study area (Figure 8b). The western sites dominate in Sp_3, where *WPD* decreases from west to east (Figure 8c). The *WPD* pattern of Sp_4 suggests that the elevated areas of the Black Forest – the largest and highest low mountain range in the study area, located in the southwest – as well as the offshore sites in the Baltic Sea, exhibit the highest *WPD* values in this component (Figure 8d).

The patterns of Sp_2 to Sp_4 are interpreted as either amplifying or attenuating Sp_1. For example, in Sp_2, the southwestern wind turbine sites contribute most strongly to the amplification of Sp_1. In Sp_4, the highly elevated sites in the southwestern low mountain ranges and the offshore sites in the northeast of the study area contribute most to this amplification.

 doi:10.20944/preprints202506.2335.v1

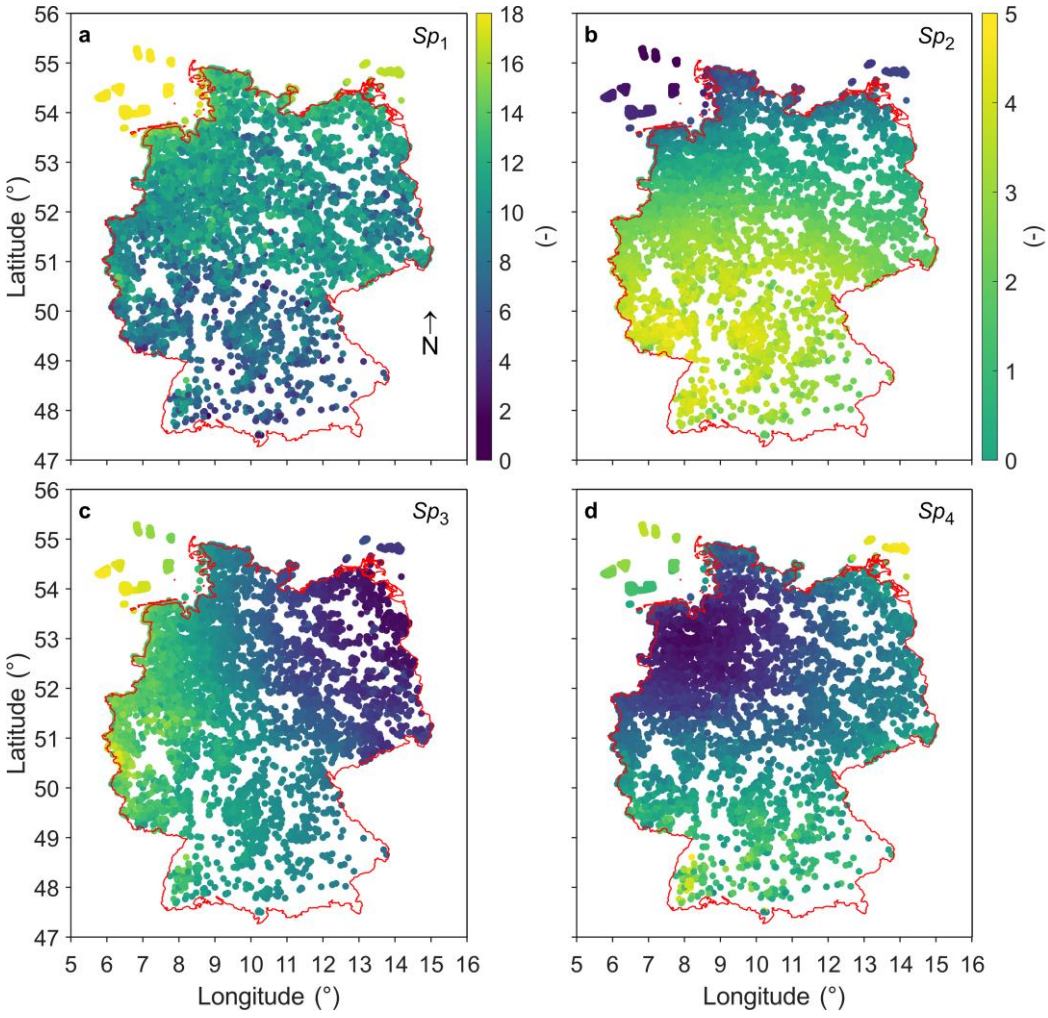

Figure 8. Spatial pattern (Sp_k, k = 1, …, 4) associated with the four singular value decomposition (SVD) components (**a**) Sp_1, (**b**) Sp_2, (**b**) Sp_3, and (**d**) Sp_4 in the study area 2015-2024. The colorbar next to subfigure (b) also applies to subfigure (c) and (d).

The wind turbine sites that behave complementarily to Sp_1 are shown in Figure 9. All wind turbine sites that do not contribute to the amplification of Sp_1 are not displayed. For SpC_2, this includes all offshore and onshore turbines located in the northernmost part of the study area (Figure 9a). These turbines do not contribute to Sp_1 because Sp_2 is negative for them and Sp_1 dominates. Toward the south, the complementary contribution of wind turbines to Sp_1 increases. The highest contributions – those exceeding the 90th percentile (P_{90}) – are provided by turbines located in the southwestern part of the study area.

A completely different pattern emerges for the complementary contributions from Sp_3. Wind turbines located in the western part of the study area provide the highest complementary contributions to Sp_1 (Figure 9b). Turbines located in the eastern part make no complementary contribution to Sp_1.

For the complementary contributions from Sp_4, a pattern emerges that is oriented toward the south and east (Figure 9c). In this component, wind turbines located in the south and offshore in the northeast contribute most strongly to the amplification of Sp_1. All onshore turbines in the northwest provide no complementary contributions, as Sp_1 also dominates at their sites.

The reduction of site-specific *WPD* time series to a few SVD components enables rapid, large-scale assessment for further planning of wind energy expansion. It immediately becomes apparent which parts of the study area are suitable for the development of complementary sites. This implies that sites contributing to wind energy generation at the same time are also identified. At such sites –

 doi:10.20944/preprints202506.2335.v1

for example, in the northern part near the North Sea coast – additional wind turbines significantly contribute to wind energy yield. However, their contribution is of a mostly supplementary nature, contributing to Sp_1.

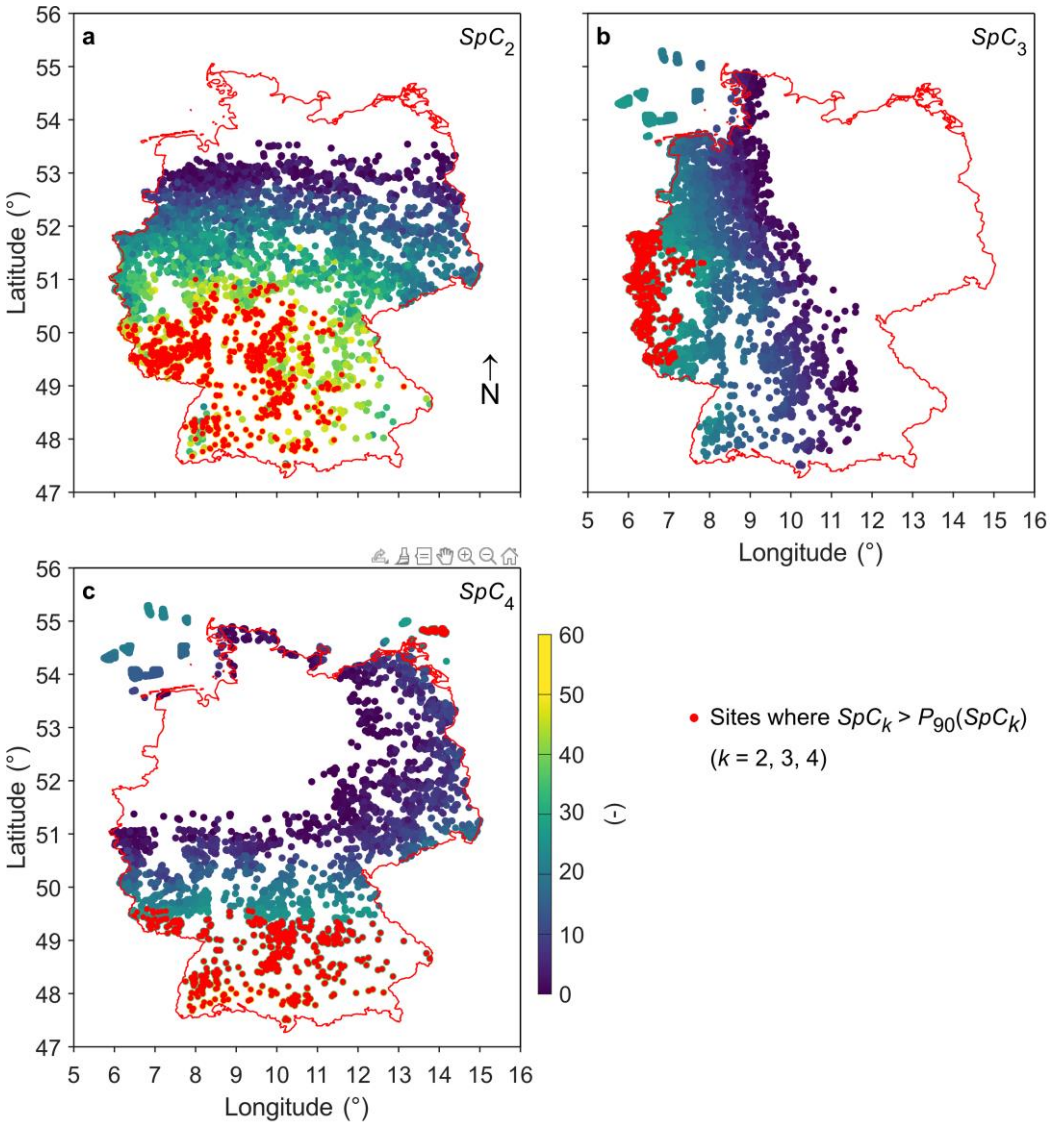

Figure 9. Complementarity ($SpC_k(i)$) of spatial patterns ($Sp_k(i)$) associated with three (k = 2, 3, 4) singular value decomposition (SVD) components at i = 1, …, 29807 wind turbine sites with $Sp_1(i)$. **(a)** $SpC_2(i)$, **(b)** $SpC_3(i)$, and **(c)** $SpC_4(i)$. Red dots indicate wind turbine sites where the complementary contribution associated with SpC_k exceeds the SVD component-specific 90th percentile.

The assumption that all wind turbine sites where $Sp_k(i)$ with a negative sign does not provide a complementary contribution to the amplification of $Sp_1(i)$ opens a wide range of possibilities for analyzing the spatiotemporal contributions of the wind turbine fleet within the study area.

For example, Figure 10a shows all turbine sites where $Te_{2,\mathrm{pos}}$ to $Te_{4,\mathrm{pos}}$ contribute only very little (combined contributions less than 20 %) to the amplification of Te_1.

As another example, Figure 10b displays all wind turbine sites where no amplification of Te_1 occurs through Te_2 to Te_4, as all of them are negative at those sites.

 doi:10.20944/preprints202506.2335.v1

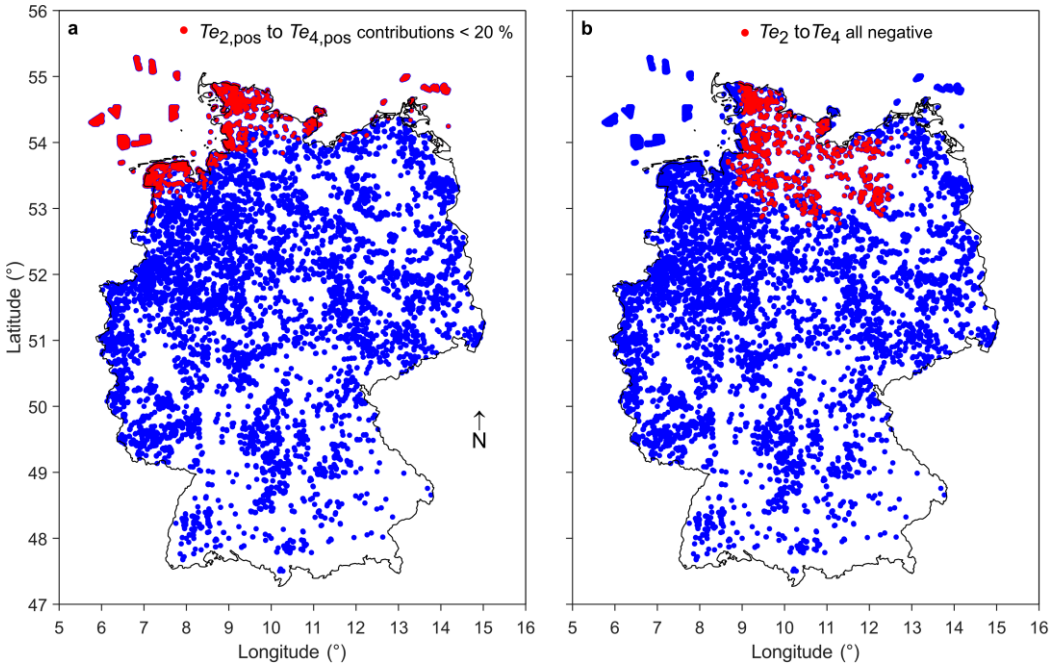

Figure 10. (**a**) Wind turbine sites where the temporal structure of singular values decomposition (SVD) components (Te_k, k = 2, 3, 4) $Te_{2,\mathrm{pos}}$ to $Te_{4,\mathrm{pos}}$ contribute only little (combined contributions less than 20 %) to the amplification of Te_1; (**b**) Wind turbine sites where Te_2 to Te_4 are all negative and do not amplify Te_1.

3.4. Spatiotemporal Pattern of Wind Power Density

The wind turbine sites at which C_2 to C_4 exceed the respective 90th percentile during the study period are shown in Figure 11. The displayed values, normalized by WiCoMo results, are given in W/m². C_2-sites contributing most strongly are located from the center of the study area down to its southern border (Figure 11a). The C_3 sites with the highest complementary contributions are found in the western part of the study area (Figure 11b). The C_4 sites with the highest contributions are situated in the south at elevated low mountain range sites and in the far northeast in the Baltic Sea (Figure 11c). The wind turbine sites in the Baltic Sea show the highest complementary contributions across all components.

 doi:10.20944/preprints202506.2335.v1

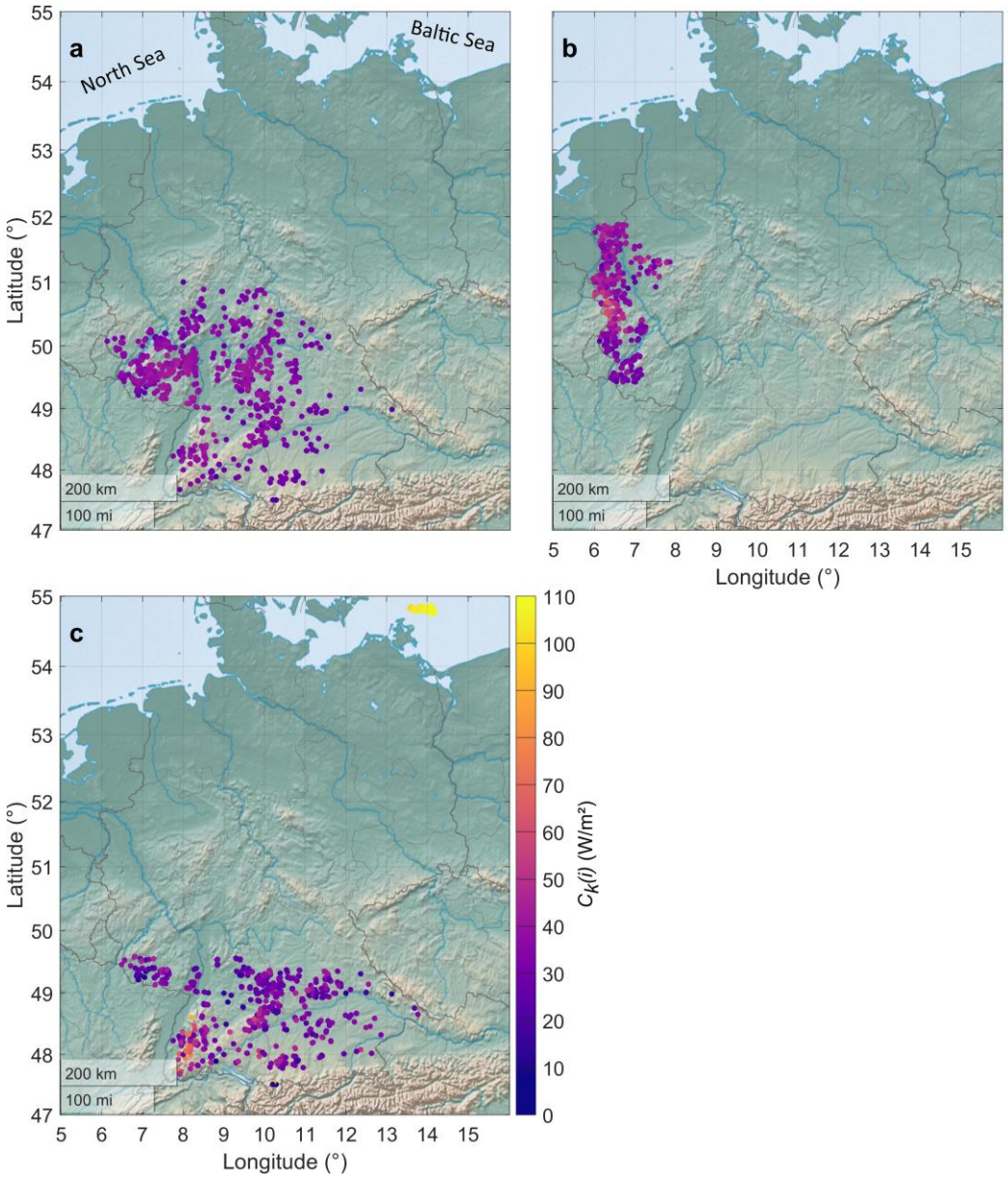

Figure 11. Mean complementary contributions exceeding the 90th percentile ($C_k(i) > P_{90}(C_k(i))$, $k = 2, 3, 4$) of components from singular value decomposition (SVD) to wind power density associated with $C_1(i)$ at wind turbine sites (i). (**a**) $C_2(i)$, (**b**) $C_3(i)$, and (**c**) $C_4(i)$ in the study area 2015-2024.

4. Conclusions

The presented results show that the combination of wavelet analysis and singular value decomposition can provide valuable and expansion-relevant information on the spatiotemporal variability of wind resources in a large area with numerous wind turbines. In contrast to correlation-based approaches, which only allow for global statistical statements on complementarity over entire time periods mostly for pairs of sites, the proposed approach enables site-specific and temporally localized assessments of complementarity for many individual operating wind turbines and candidate turbine sites.

The singular value decomposition provides valuable insights into the structure of the wind power density data. While the first component can be directly interpreted as a contribution to physical energy production, the subsequent components should be understood as modulators of the dominant pattern. Their significance lies in revealing the complexity and complementarity of the wind power patterns. They are modulation patterns: they indicate how much more or less wind power is present relative to the main structure.

 doi:10.20944/preprints202506.2335.v1

The spatial specification of complementary contributions makes it possible to identify sites where, at first glance, lower average wind speed values do not suggest a productive wind resource. Through the decomposition into components, which highlight their site-specific importance, it becomes possible to better assess the value of such sites for wind power supply, as the approach enables high-resolution temporal and spatial analyses that allow for conclusions beyond global statistical site metrics.

The area-wide overview of site characteristics and wind potentials can be used for the optimizing strategic planning of grid infrastructure, storage systems, and combined generation structures – such as hybrid wind-solar plants – since the approach is easily transferable to solar energy site assessment as well. In a resource-centered approach it helps to find zones in which the hybrid use of renewable energies should be prioritized to protect climate as efficiently as possible [87].

Author Contributions: Conceptualization, D.S.; methodology, C.J., D.S.; software, C.J., D.S.; validation, C.J., D.S.; formal analysis, D.S.; resources, D.S.; data: C.J., K.B., D.S., C.S.; data curation, C.J., D.S.; writing – original draft preparation, D.S.; writing – review and editing, C.J., K.B., L.S., C.S., D.S., J.W.; visualization, C.J., D.S.; All authors have read and agreed to the published version of the manuscript.

Funding: This research received no external funding.

Data Availability Statement: Data will be made available on request.

Acknowledgments: This research did not receive any specific grant from funding agencies in the public, commercial or not-for-profit sectors.

Conflicts of Interest: K.B. and C.S. are employed by the company Das Grüne Emissionshaus (https://www.das-gruene-emissionshaus.de/) who provided the operational wind turbine data for validation purposes. The other authors declare no conflict of interest.

Abbreviations

The following abbreviations are used in this manuscript:

a	Wavelet scaling factor
b	Wavelet translation factor
C	SVD component-specific contributions to *WPD*
EV	Variance explained by the SVD components (%)
j	Index for orthonormal SVD components
k	Index for orthonormal SVD components
K	Total number of SVD components
MAE	Mean absolute error (m/s)
N	Number of wavelet scales
ρ	Air density (kg/m³)
ψ	Mother wavelet function
P_{90}	90th percentile
R	Pearson correlation coefficient
Re	Real part of wavelet coefficients
s	Singular values
S	Matrix containing singular values
Sp	Spatial pattern of SVD components (W/m²)
SpC	Spatial complementarity
SVD	Singular value decomposition
t	Time (hour)
T	Hermitian transpose of V
Te	Temporal structure of SVD components
Te_{pos}	Positive Te values (W/m²)
u	Left singular vector, temporal mode
U	Matrix containing left singular vectors

 doi:10.20944/preprints202506.2335.v1

v	Right singular vector, temporal mode
V	Matrix containing right singular vectors
VS	Wavelet variance spectrum
W	Wavelet coefficients
WiCoMo	Wind speed complementarity model [44]
WPD	Wind power density (W/m²)
WPD_{mean}	Mean wind power density (W/m²)
WS	Wind speed (m/s)
WS_{100m}	Hourly WiCoMo wind speed at 100 m altitude (m/s)

References

1. Marquis, M.; Wilczak, J.; Ahlstrom, M.; Sharp, J.; Stern, A.; Smith, J.C.; Calvert, S. Forecasting the wind to reach significant penetration levels of wind energy. Bull. Amer. Meteorol. Soc. **2011**, *92*, 1159–1171. https://doi.org/10.1175/2011BAMS3033.1
2. Jung, C.; Schindler, D. On the inter-annual variability of wind energy generation – A case study from Germany. Appl. Energy **2018**, *230*, 845–854. https://doi.org/10.1016/j.apenergy.2018.09.019
3. Feser, F.; Krueger, O.; Woth, K.; van Garderen, L. North Atlantic winter storm activity in modern reanalyses and pressure-based observations. J. Clim. **2021**, *34*, 2411–2428. https://doi.org/10.1175/JCLI-D-20-0529.1
4. Ciria, T.P.; Puspitarini, H.D.; Chiogna, G.; François, B.; Borga, M. Multi-temporal scale analysis of complementarity between hydro and solar power along an alpine transect. Sci. Total Environ. **2020**, *741*, 140179. https://doi.org/10.1016/j.scitotenv.2020.140179
5. Martinez, A.; Iglesias, G. Hybrid wind-solar energy resources mapping in the European Atlantic. Sci. Total Environ. **2024**, *928*, 172501. https://doi.org/10.1016/j.scitotenv.2024.172501
6. Cortesi, N.; Torralba, V.; González-Reviriego, N.; Soret, A.; Doblas-Reyes.; F.J. Characterization of European wind speed variability using weather regimes. Clim. Dyn. **2019**, *534*, 961–976. https://doi.org/10.1007/s00382-019-04839-5
7. Garrido-Perez, J.M.; Ordóñez, C.; Barriopedro, D.; García-Herrera, R.; Paredes, D. Impact of weather regimes on wind power variability in western Europe. Appl. Energy **2020**, *264*, 114731. https://doi.org/10.1016/j.apenergy.2020.114731
8. Drücke, J.; Borsche, M.; James, P.; Kaspar, F.; Pfeifroth, U.; Ahrens, B.; Trentmann, J. Climatological analysis of solar and wind energy in Germany using the Grosswetterlagen classification. Renew. Energy **2021**, *164*, 1254–1266. https://doi.org/10.1016/j.renene.2020.10.102
9. Mejia, A.H.; Brouwer, J.; Copp, D.A. Performance and dynamics of California offshore wind alongside Western US onshore wind and solar power. Renew. Energy Focus **2023**, *47*, 100490. https://doi.org/10.1016/j.ref.2023.100490
10. Krakauer, N.Y.; Cohan, D.S. Interannual variability and seasonal predictability of wind and solar resources. Resources **2017**, *6*, 29. https://doi.org/10.3390/resources6030029
11. Schindler, D.; Schmidt-Rohr, S.; Jung, C. On the spatiotemporal complementarity of the European onshore wind resource. Energy Convers. Manage. **2021**, *237*, 114098. https://doi.org/10.1016/j.enconman.2021.114098
12. Holt, E.; Wang, J. Trends in wind speed at wind turbine height of 80 m over the contiguous United States using the North American Regional Reanalysis (NARR). J. Appl. Meteorol. Climatol. **2012**, *51*, 2188–2202. https://doi.org/10.1175/JAMC-D-11-0205.1
13. Wohland, J.; Omrani, N.-E.; Witthaut, D.; Keenlyside, N.S. Inconsistent wind speed trends in current twentieth century reanalyses. J. Geophys. Res. Atmos. **2019**, *124*, 1931–1940. https://doi.org/10.1029/2018JD030083
14. Schindler, D.; Behr, H.D.; Jung, C. On the spatiotemporal variability and potential of complementarity of wind and solar resources. Energy Convers. Manage. **2020**, *218*, 113016. https://doi.org/10.1016/j.enconman.2020.113016
15. Miao, H.; Xu, H.; Yang, K.; Tang, H.; Deng, J.; Xu, M.; Ning, G.; Huang, G. The reversal of surface wind speed trend in Northeast China: impact from aerosol emissions. Clim. Dyn. **2025**, *63*, 43. https://doi.org/10.1007/s00382-024-07544-0

 doi:10.20944/preprints202506.2335.v1

16. Sun, Q.; Che, J.; Hu, K.; Qin, W. Deterministic and probabilistic wind speed forecasting using decomposition methods: Accuracy and uncertainty. Renew. Energy **2025**, *243*, 122515. https://doi.org/10.1016/j.renene.2025.122515
17. Jung, C.; Schindler, D. The annual cycle and intra-annual variability of the global wind power distribution estimated by the system of wind speed distributions. Sust. Energ. Techn. Assess. **2020**, *42*, 100852. https://doi.org/10.1016/j.seta.2020.100852
18. Grams, C.M.; Beerli, R.; Pfenninger, S.; Staffell, I.; Wernli, H. Balancing Europe's wind-power output through spatial deployment informed by weather regimes. Nat. Clim. Change **2017**, *7*, 557–562. https://doi.org/10.1038/nclimate3338
19. Mockert, F.; Grams, C.M.; Brown, T.; Neumann, F. Meteorological conditions during periods of low wind speed and insolation in Germany: The role of weather regimes. Meteorol. Appl. **2023**, *30*, e2141. https://dx.doi.org/10.1002/met.2141
20. Hart, E.K.; Stoutenberg, E.D.; Jacobson, M.Z. The potential of intermittent renewables to meet electric power demand: Current methods and emerging analytical techniques. Proc. IEEE **2012**, *100*, 322–334. https://doi.org/10.1109/JPROC.2011.2144951
21. Raynaud, D.; Hingray, B.; François, B.; Creutin, J.D. Energy droughts from variable renewable energy sources in European climates. Renew. Energy **2018**, *125*, 578–589. https://doi.org/10.1016/j.renene.2018.02.130
22. Weber, J.; Wohland, J.; Reyers, M.; Moemken, J.; Hoppe, C.; Pinto, J.G.; Witthaut, D. Impact of climate change on backup energy and storage needs in wind-dominated power systems in Europe. PLoS ONE **2018**, *13*, e0201457. https://doi.org/10.1371/journal.pone.0201457
23. Bloomfield, H.C.; Brayshaw, D. J.; Troccoli, A.; Goodess, C.M.; De Felice, M.; Dubus, L.; Bett, P.E.; Saint-Drenan, Y.M. Quantifying the sensitivity of European power systems to energy scenarios and climate change projections. Renew. Energy **2021**, *164*, 1062–1075. https://doi.org/10.1016/j.renene.2020.09.125
24. Jung, C.; Schindler, D. Development of onshore wind turbine fleet counteracts climate change-induced reduction in global capacity factor. Nat. Energy **2022**, *7*, 608–619. https://doi.org/10.1038/s41560-022-01056-z
25. Leahy, P.G.; McKeogh, E.J. Persistence of low wind speed conditions and implications for wind power variability. Wind Energy **2013**, *16*, 575–586. https://doi.org/10.1002/we.1509
26. Handschy, M.A.; Rose, S.; Apt, J. Is it always windy somewhere? Occurrence of low-wind-power events over large areas. Renew. Energy **2017**, *101*, 1124–1130. https://doi.org/10.1016/j.renene.2016.10.004
27. Engeland, K.; Borga, M.; Creutin, J.D.; François, B.; Ramos, M.H.; Vidal, J.P. Space-time variability of climate variables and intermittent renewable electricity production–A review. Renew. Sustain. Energy Rev. **2017**, *79*, 600–617. https://doi.org/10.1016/j.enconman.2023.117575
28. Kahn, E. The reliability of distributed wind generators. Electr. Pow. Syst. Res. **1979**, *2*, 1-14. https://doi.org/10.1016/0378-7796(79)90021-X
29. Takle, E.S.; Shaw, R.H. Complimentary nature of wind and solar energy at a continental mid-latitude station. Int. J. Energ. Res. **1979**, *3*, 103–112. https://doi.org/10.1002/er.4440030202
30. Jurasz, J.; Canales, F.A.; Kies, A.; Guezgouz, M.; Beluco, A. A review on the complementarity of renewable energy sources: Concept, metrics, application and future research directions. Sol. Energy **2020**, *195*, 703–724. https://doi.org/10.1016/j.solener.2019.11.087
31. Malvaldi, A.; Weiss, S.; Infield, D.; Browell, J.; Leahy, P.; Foley, A.M. A spatial and temporal correlation analysis of aggregate wind power in an ideally interconnected Europe. Wind Energy **2017**, *20*, 1315–1329. https://doi.org/10.1002/we.2095
32. Heide, D.; von Bremen, L.; Greiner, M.; Hoffmann, C.; Speckmann, M.; Bofinger, S. Seasonal optimal mix of wind and solar power in a future, highly renewable Europe. Renew. Energy **2010**, *35*, 2483–2489. https://doi.org/10.1016/j.renene.2010.03.012
33. Monforti, F.; Gaetani, M.; Vignati, E. How synchronous is wind energy production among European countries? Renew. Sust. Energy Rev. **2016**, *59*, 1622–1638. https://dx.doi.org/10.1016/j.rser.2015.12.318
34. Viviescas, C.; Lima, L.; Diuana, F.A.; Vasquez, E.; Ludovique, C.; Silva, G.N.; Huback, V.; Maglar, L.; Szklo, A.; Lucena, A.F.P.; Schaeffer, R.; Paredes, J.R. Contribution of Variable Renewable Energy to increase

 doi:10.20944/preprints202506.2335.v1

energy security in Latin America: Complementarity and climate change impacts on wind and solar resources. Renew. Sustain. Energy Rev. **2019**, *113*, 109232. https://doi.org/10.1016/j.rser.2019.06.039

35. Canales, F.A.; Jurasz, J.; Beluco, A.; Kies, A. Assessing temporal complementarity between three variable energy sources through correlation and compromise programming. Energy **2020**, *192*, 116637. https://doi.org/10.1016/j.energy.2019.116637
36. Gallardo, R.P.; Ríos, A.M.; Ramírez, J.S. Analysis of the solar and wind energetic complementarity in Mexico. J. Clean. Prod. **2020**, *268*, 122323. https://doi.org/10.1016/j.jclepro.2020.122323
37. Henao, F.; Viteri, J.P.; Rodríguez, Y.; Gómez, J.; Dyner, I. Annual and interannual complementarities of renewable energy sources in Colombia. Renew. Sust. Energy Rev. **2020**, *134*, 110318. https://doi.org/10.1016/j.rser.2020.110318
38. Couto, A.; Estanqueiro, A. Assessment of wind and solar PV local complementarity for the hybridization of the wind power plants installed in Portugal. J. Clean. Prod. **2021**, *319*, 128728. https://doi.org/10.1016/j.jclepro.2021.128728
39. Gao, Y.; Ma, S.; Wang, T.; Miao, C.; Yang, F. Distributed onshore wind farm siting using intelligent optimization algorithm based on spatial and temporal variability of wind energy. Energy **2022**, *258*, 124816. https://doi.org/10.1016/j.energy.2022.124816
40. Hou, W.; Zhang, X.; Wu, M.; Feng, Y.; Yang, L. Integrating stability and complementarity to assess the accommodable generation potential of multiscale solar and wind resources: A case study in a resource-based area in China. Energy **2022**, *261*, 125312. https://doi.org/10.1016/j.energy.2022.125312
41. Lv, A.; Li, T.; Zhang, W.; Liu, Y. Spatiotemporal distribution and complementarity of wind and solar energy in China. Energies, **2022**, *15*, 7365. https://doi.org/10.3390/en15197365
42. Couto, A.; Estanqueiro, A. Wind power plants hybridised with solar power: A generation forecast perspective. J. Clean. Prod. **2023**, 423, 138793. https://doi.org/10.1016/j.jclepro.2023.138793
43. Magaña-González, R.C.; Rodriguez-Hernandez, O.; Canul-Reyes, D.A. Analysis of seasonal variability and complementarity of wind and solar resources in Mexico. Sustain. Energy Technol. Assess. **2023**, *60*, 103456. https://doi.org/10.1016/j.seta.2023.103456
44. Jung, C.; Schindler, D. Introducing a new wind speed complementarity model. Energy **2023**, *265*, 126284. https://doi.org/10.1016/j.energy.2022.126284
45. Prol, J.L.; de Llano Paz, F.; Calvo-Silvosa, A.; Pfenninger, S.; Staffell, I. Wind-solar technological, spatial and temporal complementarities in Europe: A portfolio approach. Energy **2024**, *292*, 130348. https://doi.org/10.1016/j.energy.2024.130348
46. Lv, F.; Tang, H. Assessing the impact of climate change on the optimal solar–wind hybrid power generation potential in China: A focus on stability and complementarity. Renew. Sust. Energy Rev. **2025**, *212*, 115429. https://doi.org/10.1016/j.rser.2025.115429
47. Gonzalez-Salazar, M.; Poganietz, W.R. Evaluating the complementarity of solar, wind and hydropower to mitigate the impact of El Niño Southern Oscillation in Latin America. Renew. Energy **2021**, *174*, 453-467. https://doi.org/10.1016/j.renene.2021.04.048
48. Guezgouz, M.; Jurasz, J.; Chouai, M.; Bloomfield, H.; Bekkouche, B. Assessment of solar and wind energy complementarity in Algeria. Energy Convers. Manage. **2021**, *238*, 114170. https://doi.org/10.1016/j.enconman.2021.114170
49. Jurasz, J.; Mikulik, J.; Dąbek, P.B.; Guezgouz, M.; Kaźmierczak, B. Complementarity and 'resource droughts' of solar and wind energy in Poland: An ERA5-based analysis. Energies **2021**, *14*, 1118. https://doi.org/10.3390/en14041118
50. Jurasz, J.; Guezgouz, M.; Campana, P.E.; Kaźmierczak, B.; Kuriqi, A.; Bloomfield, H.; Hingray, B.; Canales, F.A.; Hunt, J.D.; Sterl, S.; Elkadeem, M.R. Complementarity of wind and solar power in North Africa: Potential for alleviating energy droughts and impacts of the North Atlantic Oscillation. Renew. Sust. Energy Rev. **2024**, *191*, 114181. https://doi.org/10.1016/j.rser.2023.114181
51. Canul-Reyes, D.A.; Rodríguez-Hernández, O.; Barragán-Peña, M.E.; del Rio, J.A. Analysis of offshore wind energy and solar photovoltaic production and its relationship with regional electricity demand in the Yucatan peninsula. Energy **2025**, *314*, 134060. https://doi.org/10.1016/j.energy.2024.134060

 doi:10.20944/preprints202506.2335.v1

52. Meng, J.; Dong, Z.; Zhu, S. A copula-based wind-solar complementarity coefficient: Case study of two clean energy bases, China. Energy **2025**, *318*, 134904. https://doi.org/10.1016/j.energy.2025.134904
53. Han, S.; Zhang, L.N.; Liu, Y.-Q.; Zhang, H.; Yan, J.; Li, L.; Lei, X.-H.; Wang, X. Quantitative evaluation method for the complementarity of wind–solar–hydro power and optimization of wind–solar ratio. Appl. Energy **2019**, *236*, 973–984. https://doi.org/10.1016/j.apenergy.2018.12.059
54. Ren, G.; Wan, J.; Liu, J.; Yu, D. Spatial and temporal assessments of complementarity for renewable energy resources in China. Energy **2019**, *177*, 262-275. https://doi.org/10.1016/j.energy.2019.04.023
55. Ren, G.; Wan, J.; Liu, J.; Yu, D. Spatial and temporal correlation analysis of wind power between different provinces in China. Energy **2020**, *191*, 116514. https://doi.org/10.1016/j.energy.2019.116514
56. Ren, G.; Wang, W.; Wan, J.; Hong, F.; Yang, K. A novel metric for assessing wind and solar power complementarity based on three different fluctuation states and corresponding fluctuation amplitudes. Energy Convers. Manage. **2023**, *278*, 116721. https://doi.org/10.1016/j.enconman.2023.116721
57. Kapica, J.; Canales, F.A.; Jurasz, J. Global atlas of solar and wind resources temporal complementarity. Energy Convers. Manage. **2021**, *246*, 114692. https://doi.org/10.1016/j.enconman.2021.114692
58. Jani, H.K.; Kantipudi, M.V.V.P.; Nagababu, G.; Prajapati, D.; Kachhwaha, S.S. Simultaneity of wind and solar energy: A spatio-temporal analysis to delineate the plausible regions to harness. Sustain. Energy Technol. Assess. **2022**, *53*, 102665. https://doi.org/10.1016/j.seta.2022.102665
59. Delbecke, O.; Moschner, J.D.; Driesen, J. The complementarity of offshore wind and floating photovoltaics in the Belgian North Sea, an analysis up to 2100. Renew. Energy **2023**, *218*, 199253. https://doi.org/10.1016/j.renene.2023.119253
60. Li, P.; Lian, J.; Ma, C.; Zhang, J. Complementarity and development potential assessment of offshore wind and solar resources in China seas. Energy Convers. Manage. **2023**, *296*, 117705. https://doi.org/10.1016/j.enconman.2023.117705
61. Fang, W.; Yang, C.; Liu, D.; Huang, Q.; Ming, B.; Cheng, L.; Wang, L.; Feng, G.; Shang, J. Assessment of wind and solar power potential and their temporal complementarity in China's Northwestern provinces: insights from ERA5 reanalysis. Energies, **2023**, *16*, 7109. https://doi.org/10.3390/en16207109
62. Sun, Y.; Li, Y.; Wang, R.; Ma, R. Assessing the national synergy potential of onshore and offshore renewable energy from the perspective of resources dynamic and complementarity. Energy **2023**, *279*, 128106. https://doi.org/10.1016/j.energy.2023.128106
63. Cai, Q.; Qing, J.; Zhong, C.; Xu, Q.; Liang, Q.-M. Temporal and spatial heterogeneity analysis of wind and solar power complementarity and source-load matching characteristics in China. Energy Convers. Manage. **2024**, *315*, 118770. https://doi.org/10.1016/j.enconman.2024.118770
64. Chen, Z.; Li, W.; Wang, X.; Bai, J.; Wang, X.; Guo, J. Evaluating wind and solar complementarity in China: Considering climate change and source-load matching dynamics. Energy **2024**, *312*, 133485. https://doi.org/10.1016/j.energy.2024.133485
65. Hajou, A.; El Mghouchi, Y.; Chaoui, M. Novel approaches for wind speed evaluating and solar-wind complementarity assessing. Renew. Energy Focus **2024**, *48*, 100547. https://doi.org/10.1016/j.ref.2024.100547
66. Frías-Paredes, L.; Gastón-Romeo, M. A new methodology to easy integrate complementarity criteria in the resource assessment process for hybrid power plants: Offshore wind and floating PV. Energy Convers. Manage. X **2025**, *26*, 100938. https://doi.org/10.1016/j.ecmx.2025.100938
67. Xu, L.; Wang, Z.; Liu, Y. The spatial and temporal variation features of wind-sun complementarity in China. Energy Convers. Manage. **2017**, *154*, 138-148. http://dx.doi.org/10.1016/j.enconman.2017.10.031
68. Cantor, D.; Ochoa, A.; Mesa, O. Total variation-based metrics for assessing complementarity in energy resources time series. Sustainability **2022**, *14*, 8514. https://doi.org/10.3390/su14148514
69. Miglietta, M.M.; Huld, T.; Monforti-Ferrario, F. Local complementarity of wind and solar energy resources over Europe: an assessment study from a meteorological perspective. J. Appl. Meteorol. Climatol. **2017**, *56*, 217–234. https://dx.doi.org/10.1175/JAMC-D-16-0031.1
70. Jung, C.; Schindler, D. Projections of energy yield- and complementarity-driven wind energy expansion scenarios in the European Union. Energy Convers. Manage. **2022**, *269*, 116160. https://doi.org/10.1016/j.enconman.2022.116160

 doi:10.20944/preprints202506.2335.v1

71. Guo, Y.; Ming, B.; Huang, Q.; Yang, Z.; Kong, Y.; Wang, X. Variation-based complementarity assessment between wind and solar resources in China. Energy Convers. Manage. **2023**, *278*, 116726. https://doi.org/10.1016/j.enconman.2023.116726
72. Li, K.; Duan, P.; Yue, Q.; Cheng, Y.; Hua, J.; Chen, J.; Guo, P. Enhancing reliability assessment in distributed generation networks: Incorporating dynamic correlation of wind-solar power output uncertainty. Sustain. Energy Grids Netw. **2024**, *39*, 101505. https://doi.org/10.1016/j.segan.2024.101505
73. Shen, L.; Wang, Q.; Wan, Y.; Xu, X.; Liu, Y. Multi-timescale scheduling optimization of cascade hydro-solar complementary power stations considering spatio-temporal correlation. Sci. Technol. Energy Transit. **2025**, *80*, 17. https://doi.org/10.2516/stet/2024104
74. Berger, M.; Radu, D.; Fonteneau, R.; Henry, R.; Glavic, M.; Fettweis, X.; Le Du, M.; Panciatici, P.; Balea, L.; Ernst, D. Critical time windows for renewable resource complementarity assessment. Energy **2020**, *198*, 117308. https://doi.org/10.1016/j.energy.2020.117308
75. Campos, R.A.; do Nascimento, L.R.; Rüther, R. The complementary nature between wind and photovoltaic generation in Brazil and the role of energy storage in utility-scale hybrid power plants. Energy Convers. Manage. **2020**, *221*, 113160. https://doi.org/10.1016/j.enconman.2020.113160
76. Luz, T.; Moura, P. 100% Renewable energy planning with complementarity and flexibility based on a multi-objective assessment. Appl. Energy **2019**, *255*, 113819. https://doi.org/10.1016/j.apenergy.2019.113819
77. Moukam, T.D.T.; Sugawara, A.; Li, Y.; Bello, Y. Evaluation of power system stability for a hybrid power plant using wind speed and cloud distribution forecasts. Energies **2025**, *18*, 1540. https://doi.org/10.3390/en18061540
78. Mlilo, N.; Brown, J.; Ahfock, T. Impact of intermittent renewable energy generation penetration on the power system networks – A review. Technol. Econ. Smart Grids Sustain. Energy **2021**, *6*, 25. https://doi.org/10.1007/s40866-021-00123-w
79. Shahzad, S.; Alsenani, T.R.; Alrumayh, O.; Altamimi, A.; Kilic, H. Adaptive hydrogen buffering for enhanced flexibility in constrained transmission grids with integrated renewable energy system. Int. J. Hydro. Energy **2025**, *122*, 103962. https://doi.org/10.1016/j.erss.2025.103962
80. Siddique, M.B.; Thakur, J. Assessment of curtailed wind energy potential for off-grid applications through mobile battery storage. Energy **2020**, *201*, 117601. https://doi.org/10.3390/en16145390
81. Thomaidis, N.S.; Santos-Alamillos, F.J.; Pozo-Vázquez, D.; Usaola-García, J. Optimal management of wind and solar energy resources. Comp. Oper. Res. **2016**, *66*, 284–291. https://doi.org/10.1016/j.cor.2015.02.016
82. Wörman, A.; Pechlivanidis, I.; Mewes, D.; Riml, J.; Bertacchi Uvo, C. Spatiotemporal management of solar, wind and hydropower across continental Europe. Comms. Eng. **2024**, *3*, 3. https://doi.org/10.1038/s44172-023-00155-3
83. Xiong, H.; Xu, B.; Kheav, K.; Luo, X.; Zhang, X.; Patelli, E.; Chen, D. Multiscale power fluctuation evaluation of a hydro-wind-photovoltaic system. Renew. Energy **2021**, *175*, 153–166. https://doi.org/10.1016/j.renene.2021.04.095
84. Wilks, D.S. Statistical Methods in the Atmospheric Sciences, 4th ed.; Elsevier: Amsterdam, Netherlands, **2019**; pp. 576–577.
85. Sander, L.; Jung, C.; Schindler, D. New concept of renewable energy priority zones for efficient onshore wind and solar expansion. Energy Convers. Manage. **2023**, *294*, 117575. https://doi.org/10.1016/j.enconman.2023.117575
86. Torrence, C.; Compo, G.P. A practical guide to wavelet analysis. Bull. Am. Meteor. Soc. **1998**, *97*, 61–78. https://doi.org/10.1175/1520-0477(1998)079<0061:APGTWA>2.0.CO;2
87. Torrence, C.; Webster, P.J. Interdecadal changes in the ENSO-monsoon system. J. Clim. **1999**, *12*, 2679–2690. https://doi.org/10.1175/1520-0442(1999)012<2679:ICITEM>2.0.CO;2
88. Schindler, D.; Sander, L.; Jung, C. Importance of renewable resource variability for electricity mix transformation: A case study from Germany based on electricity market data. J. Clean. Prod. **2022**, *379*, 134728. https://doi.org/10.1016/j.jclepro.2022.134728
89. Heppelmann, T.; Steiner, A.; Vogt, S. Application of numerical weather prediction in wind power forecasting: Assessment of the diurnal cycle. Meteorol. Z. **2017**, *26*, 319–331. https://doi.org/10.1127/metz/2017/0820

 doi:10.20944/preprints202506.2335.v1

90. Petrik, R.; Geyer, B.; Rockel, B. On the diurnal cycle and variability of winds in the lower planetary boundary layer: evaluation of regional reanalyses and hindcasts. Tellus A **2021**, *73*, 1–28. https://doi.org/10.1080/16000870.2020.1804294
91. Jung, C.; Schindler, D. Introducing a new hazard and exposure atlas for European winter storms. Sci. Total Environ. **2024**, *929*, 172566. https://doi.org/10.1016/j.scitotenv.2024.172566
92. Collins, S.; Deane, P.; Gallachóir, B.Ó.; Pfenninger, S.; Staffell, I. Impacts of inter-annual wind and solar variations on the European power system. Joule **2018**, *2*, 2076–2090. https://doi.org/10.1016/j.joule.2018.06.020
93. Pryor, S.C.; Shepard, T.J.; Barthelmie, R.J. Interannual variability of wind climates and wind turbine annual energy production. Wind Energ. Sci. **2018**, *3*, 651–655. https://doi.org/10.5194/wes-3-651-2018